Base treated H-mordenite as stable catalyst in alkylbenzene transalkylation

Shang-Tien Tsai, Chien-Hao Chen and Tseng-Chang Tsai*

Received 24th March 2009, Accepted 3rd June 2009
First published as an Advance Article on the web 1st July 2009
DOI: 10.1039/b905744g

The effect of post treatment methods on the pore structure of hierarchical mordenite and its catalytic performance in transalkylation of heavy alkylbenzenes were studied. While the catalytic stability of H-mordenite deteriorated with dealumination by acid or steam treatment, it was improved with desilication by base post treatment. Comparing to the state-of-the-art Pt/mordenite catalysts, the desilicated H-mordenite showed comparable stability giving the best benzene product purity at lower hydrogen and energy consumption and presented the greenest solution. The improved stability is attributed to an enhanced diffusion behavior in the meso-micro hierarchical structure. As confirmed by NMR and sorption data, base treatment can preferentially remove framework silica and re-insert octahedral aluminium into the mordenite structure simultaneously, through which it created enlarged mesopores and defected 12-MR micropores to form a hierarchical porous structure.

1. Introduction

Aromatics are carcinogenic compounds of great concern for public health. The increasing stringent specification for reformulated gasoline has reduced the aromatics content, leading to a substantial release of heavy alkylbenzenes from reforming gasoline blending stocks. There is an increasing incentive for the petrochemical industry to convert the surplus heavy alkylbenzenes by transalkylation into benzene and xylene.[1,2] Relocating heavy alkylbenzenes can not only improve gasoline quality but also reduce the production cost of benzene and xylene.

Heavy alkylbenzenes are potent coke precursors. Transalkylation of heavy alkylbenzenes with conventional H-form zeolite catalysts exhibited fast deactivation. As it has been demonstrated in many newly industrialized processes, the long term stability of heavy alkylbenzene transalkylation catalysts can be enhanced by incorporating metals on the zeolite (metal/zeolite) through hydrogenation of coke precursors.[3–5] Nevertheless, the metal/zeolite catalysts can also catalyze the hydrogenation of aromatics causing a product purity problem. Particularly, the benzene hydrogenation produces methylcyclopentane (MCP) and cyclohexane (CH). The boiling point of MCP or CH is close to that of benzene, so called co-boilers. These byproducts could contaminate benzene leading to a deteriorated product purity in a typical distillation operation.[3]

Dealumination is a widely used post treatment method to improve the catalytic stability of zeolites in acid catalyzed reactions, for example, mesopore embedded mordenite in cumene synthesis[6] and dealuminated mordenite with steam and acid treatment in linear alkylbenzene synthesis.[7] The improved stability was attributed to the formation of secondary mesopores on mordenite.

Many new methods by means of direct synthesis or post treatment have been developed recently to prepare hierarchical zeolite.[8–11] Base treatment by adjusting alkaline solution concentration, post treating temperature and time, and parent zeolite compositions[12,13] can modify the crystal morphology[14] and selectively remove silica from the zeolitic framework. Desilication is more effective than the conventional dealumination for mesopore formation.[15,16] The catalytic properties of MFI zeolites, including aluminosilicate ZSM-5 and titanosilicate TS-1, can be improved by desilication.[17,18] The present study explores the potential application of mesoporous mordenite in the transalkylation of heavy alkylbenzenes. The effect of the pore structure prepared either by the conventional dealumination method or the new desilication method was studied.

2. Experimental

Zeolon 100 powder (denoted as M7) with a SiO_2/Al_2O_3 ratio of 6.8 supplied by Norton Chemicals was used as the parent mordenite sample. A M7 sample was subjected to various post treatments. The steam treated sample, denoted as SteamM7, was prepared from M7 by treatment with water saturated nitrogen at 25 ml min^{-1} g^{-1} catalyst at 873 K for 6 h. The acid treated sample, denoted as AcidM7, was prepared by refluxing an M7 sample in a 6 N HCl solution at a solution-to-solid ratio of 20 w/w at 363 K for 16 h. The solid was then filtrated and washed with water until the filtrate reached a pH of 7.0 and was free of chloride ions, as detected by $AgNO_3$ solution. The base treated sample, denoted as BaseM7, was prepared by heating an M7 sample in a 0.1 N NaOH solution at a solution-to-solid weight ratio of 20 w/w at 333 K for 30 minutes. The solid was then further ion exchanged with a 1 N NH_4NO_3 solution at 333 K for 6 h. A platinum incorporated mordenite sample containing 700 ppm

Department of Applied Chemistry, National University of Kaohsiung, Kaohsiung, Taiwan, 811, R.O.C. E-mail: tctsai@nuk.edu.tw; Fax: +886 7-5919348; Tel: +886 7-5919457

Table 1 Sample notations and their preparation procedures

Sample ID	Post treatment conditions
M7	Parent H-mordenite sample
BaseM7	H-mordenite treated with 0.1 N NaOH at 333 K for 30 minutes, followed by NH_4NO_3 ion exchange at 353 K and calcination at 813 K
AcidM7	H-mordenite treated with 6 N HCl at 363 K for 16 h, followed by calcination at 813 K
SteamM7	H-mordenite treated with water saturated nitrogen at 873 K for 6 h
Pt(700)/M7	H-mordenite impregnated with H_2PtCl_6 precursor at 700 ppm

Pt, denoted as Pt(700)/M7, was prepared by impregnating the H_2PtCl_6 precursor on the parent M7 sample (Table 1).

The framework structure of the solid powder was measured with a Rigaku Multiflex X-ray diffractometer using Cu Kα radiation. Its elemental composition was analyzed by a Perkin Elmer Optima 2100 DV inductive coupling plasma (ICP-AES) spectrometer; and its skeleton framework composition was characterized by ^{27}Al NMR and ^{29}Si NMR spectra by using a Bruker Avance 300 NMR spectrometer. Nitrogen adsorption isotherm and BET surface area measurements were conducted using Micromeritics ASAP2020 at 77 K. Temperature programmed desorption (TPD) tests were conducted in a HP5890 gas chromatograph equipped with a flame ionization detector using a column packed with the zeolite samples of interest.[19]

Transalkylation reaction tests were conducted in a continuous flow fixed-bed reactor. Typical reaction conditions were: feed composition as toluene to 1,2,4-trimethylbenzene (TMB) at 50 : 50 w/w; reaction temperature: 553 K; Weight hourly space velocity (WHSV): 3.0 h^{-1}; pressure: 2068 kPa; H_2/feed ratio of 3.0 mol/mol. The reactor effluent was analyzed with gas chromatography using a methylsilicone high resolution HP-1 capillary column in accordance with the ASTM D5134 DHA method (detailed hydrocarbon analysis) from which the conversion and the benzene product's purity were determined.

The spent mordenite samples were subjected to elemental analysis. Those used samples were dissolved in a HF solution. The solution was then extracted with CH_2Cl_2 to collect residual aromatic components.[20,21] The residual aromatic sample was analyzed by GC-MS spectroscopy to determine its structure and composition.

3. Results

The X-ray diffraction spectra of the parent M7 and post treated M7 samples are shown in Fig. 1. Clearly, the mordenite framework structure remained intact in all the post treatment conditions, including in AcidM7 after being refluxed in a 6 N HCl solution for 16 h, SteamM7 after steam treatment at 873 K for 6 h and BaseM7 post treated with 0.1 N NaOH at 333 K for 30 min.

The post treated samples were subject to the measurement of ^{27}Al NMR (Fig. 2) and ^{29}Si NMR (Fig. 3) to determine their skeleton framework composition. The ^{27}Al NMR spectra of the studied samples all showed two peaks centering at 54 ppm and at 0 ppm, which correspond to framework tetrahedral aluminium (Al^{IV}) and extra-framework octahedral aluminium (Al^{VI}), respectively. The parent M7 sample and all the post treated samples contained predominantly Al^{IV} sites. As shown in Table 2, the Al^{VI} distribution in the base treated BaseM7 was much lower than in the acid treated AcidM7 and in the steam treated SteamM7.

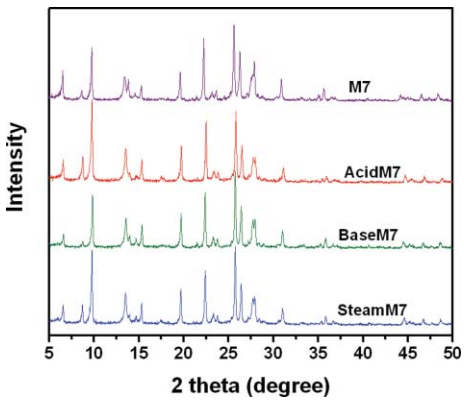

Fig. 1 X-ray diffraction spectra of parent M7 and post treated samples.

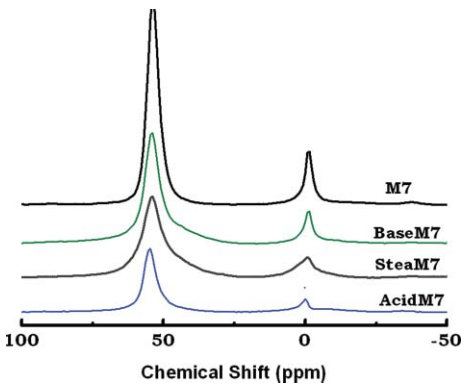

Fig. 2 ^{27}Al NMR spectra of various mordenite samples.

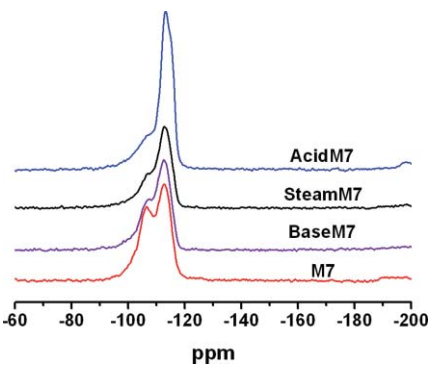

Fig. 3 ^{29}Si NMR spectra of various mordenite samples.

The framework Si/Al atomic ratio (SAR) can be determined from the population of various silicon sites in the ^{29}Si NMR spectra, which correspond to different silicon sites in different

Table 2 Physical texture properties and framework composition of parent and post treated mordenite

Sample	Si/Al (atom/atom)			Surface area/m^2 g^{-1}			Mesopore	
	ICP	NMR	Al^{VI}/Al^{IV} (%/%)	S_{BET}	S_{meso}	S_{micro}	V_{meso}/cm^3 g	Pore size/nm
M7	6.8	7.9	16.6/83.4	467.0	38.6	428.4	0.03	5.85
AcidM7	11.8	13.9	14.8/85.2	496.7	92.7	404.1	0.07	4.38
SteamM7	9.3	11.1	16.2/83.8	451.2	46.3	404.8	0.04	5.35
BaseM7	6.0	6.8	12.2/87.8	408.0	38.3	369.7	0.05	7.03

environments, *viz.*, Q^0 to Q^4 site.[22] As shown in Table 2, the SAR of the parent M7 sample determined by ICP (SAR_{ICP}) and NMR (SAR_{NMR}) are 6.8 and 7.9, respectively. The higher SAR_{NMR} than SAR_{ICP}, by 14%, in the parent M7 sample was close to the partition of Al^{VI}/Al^{IV}, 16.6%/83.4%. The SAR_{NMR} of the parent mordenite sample increased from 7.9 up to 13.9 and 11.1 in the acid treated AcidM7 and in the steam treated SteamM7, respectively. On the other hand, the base treated BaseM7 possessed a lower SAR_{NMR} of 6.8.

Fig. 4 shows the N_2 adsorption/desorption isotherms and the pore size distribution determined from desorption branch of the parent M7 sample and the post treated samples. All the tested samples exhibited Type IV isotherms with hysteresis loops of type H, indicating the existence of mesopores. The textual properties of these samples are summarized in Table 2. The parent mordenite sample M7 had a total surface area of 467.0 m^2 g^{-1} and a mesopore surface area of 38.6 m^2 g^{-1} with a pore size of 58.5 nm. All the post treatments resulted in reduced microporous surface area. Interestingly, the acid treated AcidM7 sample showed a significantly higher total surface area and a twice as high mesoporous surface area of 92.7 m^2 g^{-1} but a slightly lower mesopore size of 4.38 nm. The mesopore size of both the acid treated AcidM7 and steam treated SteamM7 was smaller than that of the parent M7 sample. In contrast, the base treated BaseM7 sample had the same mesoporous surface area but a much larger mesopore size of 7.03 nm.

The molecular size of *n*-hexane (*n*-C_6), 2-methylpentane (2MP) and 2,3-dimethylbutane (DMB) is 3.9 × 4.3 × 9.1 Å, 4.6 × 5.8 × 8.6 Å and 5.9 × 6.2 × 6.7 Å, respectively. Temperature programmed desorption (TPD) tests of those hexane isomers were used to probe the micropore structure of the various post treated mordenite samples. The desorption capacities of all the tested samples determined from the TPD curve (Fig. 5) are shown in Table 3. The TPD capacity of the parent M7 sample was 4.43%, 4.96% and 5.36% when using *n*-C_6, 2MP and DMB, respectively. While the AcidM7 and BaseM7 possessed the same desorption capacities as the parent M7 sample, the SteamM7 had lower desorption capacities for all the hexane isomers. Meanwhile, TPD peak temperatures for *n*-C_6 or DMB isomers over the tested samples increased in the order AcidM7 < BaseM7 ~ M7 < SteamM7.

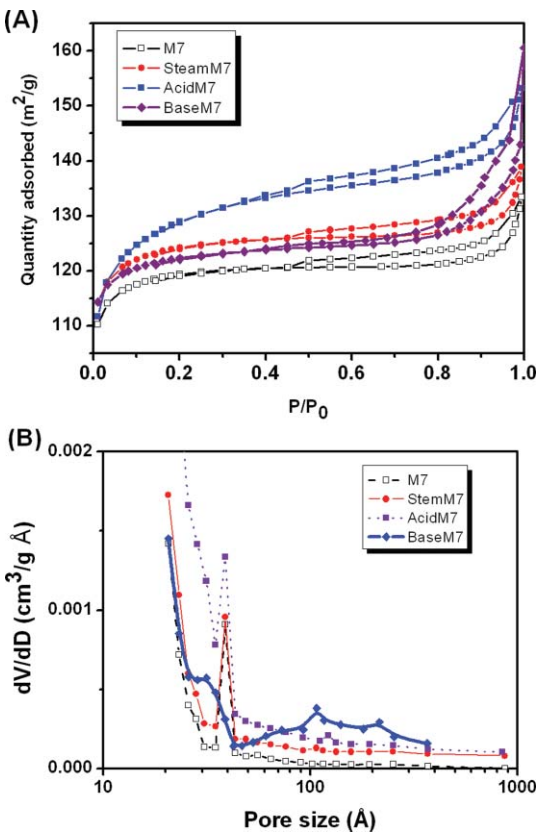

Fig. 4 BET nitrogen isotherm of various post treated mordenite samples, (A) adsorption/desorption isotherm; (B) pore size distribution.

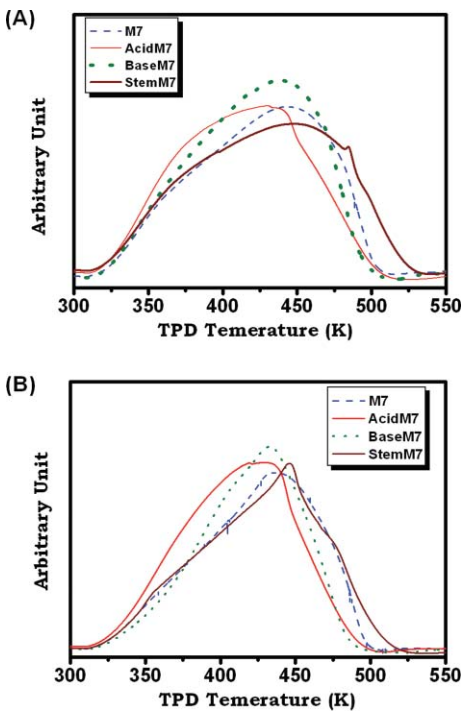

Fig. 5 Temperature programmed desorption of hexane isomers in various mordenite samples (A) *n*-hexane TPD; (B) DMB TPD.

Table 3 Adsorption capacity of hexane isomers determined by temperature programmed desorption

	Probing molecules					
	n-C_6		MP		DMB	
Sample ID	Capacity (%)	Peak T/K	Capacity (%)	Peak T/K	Capacity (%)	Peak T/K
M7	4.43	444	4.96	456	5.36	438
AcidM7	4.63	428	4.93	435	5.40	430
SteamM7	4.00	449	4.75	451	5.11	447
BaseM7	4.43	439	5.02	436	5.40	433
MCM-41	0	—	0	—	0	—

Table 4 Catalytic performances of parent M7 and post treated M7 catalyst in the transalkylation of toluene–trimethylbenzene at 50 : 50 w/w (reaction conditions: 683 K, 2480 kPa, 3.0 h^{-1} WHSV and 3.0 H_2/hydrocarbon)

Catalyst ID	M7	SteamM7	AcidM7	BaseM7	Pt(700)/M7
Time-on-stream/h	4.0	2.0	4.0	4.0	4.0
Product yield (wt%)					
C_6^- gas	0.04	0.12	1.10	0.20	0.82
Naphthenes	0	0	0	0	0.24
Benzene	2.10	3.23	3.29	2.90	1.80
Toluene	20.73	26.82	23.41	22.10	23.53
Xylene	42.49	25.42	40.22	39.88	41.92
Methylethylbenzene	0.33	0.70	0.84	1.17	0.53
Trimethylbenzene	30.26	38.68	27.35	29.19	27.37
Tetramethylbenzene	4.04	5.05	3.78	4.56	3.60
Performance					
A_{7+9} conversion (wt%)	49.0	34.5	49.2	48.7	49.1
A_{6+8} yield (wt%)	44.6	28.6	43.5	42.8	44.0
A_8/A_6 (mol/mol)	14.9	5.8	9.0	10.1	15.0
Benzene purity (%)	100.0	100.0	100.0	100.0	90.05

Transalkylation is a thermodynamically controlled reaction in which the equilibrium composition depends on the methyl/ring (M/R) ratio of reaction systems.[23] The M/R ratio of pure toluene and TMB feed is 1.0 and 3.0, respectively. With an increasing M/R ratio, in addition to xylene product, the dominant reaction product shifts from benzene to tetramethylbenzene (TEMB). The product value of TEMB is much lower than that of the most desirable benzene and xylene. Conventionally, the product value is estimated from the total yield of benzene and xylene (A_{6+8}). Maximum xylene product selectivity appears at a M/R ratio of around 2.0 for toluene–TMB mixture at equal molar ratio. On the other hand, the feed reactivity increases with increasing M/R ratio and the required reaction temperature decreases accordingly. Therefore, feed compositions at 50 : 50 w/w composition could be a representative model feed to reflect the economics as well as the activity and selectivity of a catalyst system of interest. The catalytic performances of various mordenite samples are compared using the model feed in Table 4. The parent M7 catalyst showed a total conversion of toluene and TMB of 49.0%, producing the premium A_{6+8} product yield of 44.6% and A_{10} yield of 4.04%. Comparing to the parent M7 catalyst, the acid treated sample AcidM7 and the base treated BaseM7 had comparable conversions at slightly lower A_{6+8} product yields. On the other hand, because of a high deactivation rate, steam treated SteamM7 showed a much lower conversion and product yield. At even a short time-on-stream of 2 h, its conversion was down to 34.5% giving a relatively low A_{6+8} yield of 28.6%. All the post treated M7 catalysts favored the production of benzene over xylene with a lower A_8/A_6 ratio and a slightly higher A_{10} yield, indicating that all the post treatments enhance the disproportionation of A_7 and A_9.

Fig. 6 depicts the catalytic stability of the parent M7 sample and various post treated mordenite samples in the transalkylation of the model feed. All the parent M7 and post treated samples had about the same initial activity. While the parent M7 sample quickly deactivated, the deactivation rate was slightly faster over the acid treated AcidM7 sample but severely accelerated over the steam treated SteamM7 sample. Interestingly, as shown in Fig. 6, the catalytic conversion over base treated BaseM7 was remarkably stable. Incorporating platinum in zeolite (Pt/zeolite) can effectively stabilize zeolite

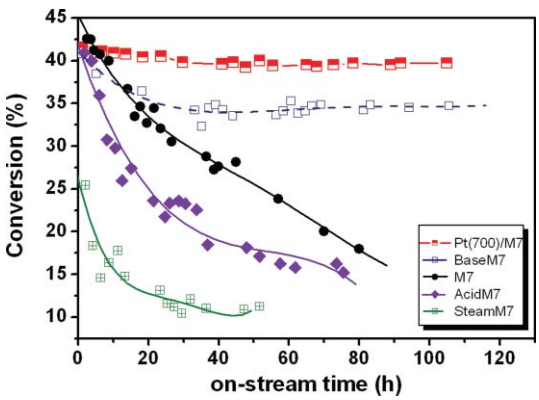

Fig. 6 Catalytic performances of various mordenite samples in transalkylation of toluene and 1,2,4-trimethylbenzene (reaction conditions: 653 K, 2480 kPa, 3.0 h^{-1} WHSV and 3.0 H_2/HC).

Table 5 Structure and composition of residual aromatics deposited on spent mordenite samples

Sample ID	M7	SteamM7	AcidM7	BaseM7	Pt(700)/M7
Residual aromatics (wt%)	4.6	5.5	4.1	5.4	5.1
H/C (atom/atom)	1.3	1.4	1.3	1.3	1.5
Component (%)					
Trimethylbenzene	100.0	95.6	100.0	100	68.8
Methylethylbenzene	0	3.7	0	0	24.9
Propylbenzene	0	0	0	0	4.8
Dimethylethylbenzene	0	0.7	0	0	1.5

activity in transalkylation of heavy alkylbenzenes.[3,24] As shown in Fig. 6, the catalytic stability of Pt(700)/M7 at a platinum content of 700 ppm was comparable to that of BaseM7. At line-out stabilized activity at time-on-stream of 100 h, the A_{6+8} yield over BaseM7 and Pt(700)/M7 was 34.7% and 40.1%, respectively. Nevertheless, as shown in Table 4, transalkylation over Pt(700)/M7 produced substantial naphthene products, such as CH and MCP, which dwindled benzene product purity down to 90.05%, as estimated using eqn (1):

$$\text{Benzene purity} = 100 \times Y_{A_6}/(Y_{A_6} + 0.1 \times Y_{C_6P} + 0.7 \times Y_{MCP} + Y_{CH} + Y_{C_7N}) \quad (1)$$

where Y_{A_6}, Y_{C_6P}, Y_{MCP}, Y_{CH} and Y_{C_7N} represent the product yield of benzene, total hexane isomers, MCP, CH and sum of methylcyclohexane and dimethylcyclopentane, respectively.

Additional treatment is needed, such as the dual bed catalyst system by selective naphthene cracking, co-feeding sulphur compounds, or pre-coking pretreatment to suppress metal activity to improve benzene product purity up to the industrial specification of 99.85%.[24–26]

The structures and compositions of residual aromatics on spent mordenite samples were determined. The contents of residual aromatics were in the vicinity of 5 wt%. As shown in Table 5, the residual aromatics deposited on those samples were mainly TMB molecules. The residual aromatics of SteamM7 contained some A_{10} compounds. On the other hand, the residual aromatics on Pt(700)/M7 included TMB and some other A_9 and A_{10} aromatic compounds.

4. Discussion

While post treatment can generate hierarchical porous structures, characterization with conventional BET isotherms, particularly elucidating the micropore structure, can be complicated by the presence of interconnected mesopores and morphology.[27,28] Qiao *et al.* reported that MCM-41 showed an equilibrium capacity in the range of 2–7 mmol g^{-1}.[29] Interestingly, as shown in Table 3, in the proposed experimental protocol measuring the desorption capacity after adsorption breakthrough, microporous zeolite samples had some TPD capacity for hexane isomers but MCM-41 had zero capacity (Table 3). Thus, hexane TPD was used to characterize the micropore structure as a complementary measurement of the BET adsorption isotherm.

The adsorption of zeolite is affected by subtle differences in the zeolite structure,[30,31] SAR,[32,33] cation type,[34] morphology and composition. Gribov *et al.* reported that with an increasing pore dimension of zeolite, the sorption energy of *n*-hexane decreases.[32] In the earlier work of R. M. Barrer, the diffusivity of 2,2-dimethylbutane in ZSM-5 seems to be slightly dependent on the chemical composition of the zeolites.[33] Adsorption measurement on zeolites with the same or similar crystal composition and morphology sometimes is not feasible. Chen *et al.* devised the so-called "adsorption index", defined as the reciprocal of the required time for reaching 2/3 of the equilibrium adsorption capacity of 2,2-dimethylbutane, as a quick and easy way to characterize the effective pore size/volume of zeolites.[31] Similarly, sorption of hexane isomers having different molecular sizes can be a quick test for probing subtle variations in micropore structures by means of desorption capacity and desorption temperature.[19]

The catalytic stability of zeolite is dependent on SAR, the existence of octahedral aluminium (Al^{VI}) and the pore size distribution which varies with post treatment methods and treating conditions. According to Dwyer *et al.*, the surface composition of dealuminated faujasite zeolite by steam/acid leaching process is more uniform with bulk composition than that by EDTA (ethylenediaminetetraacetic acid).[35] SAR_{NMR} representing the composition of framework silicon and aluminium would increase after dealumination. As confirmed with the higher SAR_{NMR} in the post treated samples, as shown in Table 2, acid treatment and steam treatment can remove aluminium preferable to silica from the parent mordenite sample M7. Acid treatment was more effective than steam treatment in dealumination, giving a higher SAR_{NMR}, 13.9 *versus* 11.1, and removal of extra-framework octahedral aluminium Al^{VI}.

Moreover, as shown in Table 2, acid post treatment raised significantly the mesoporous surface area at reduced mesopore sizes. As for microporous structures, as shown in Table 3, AcidM7 had slightly higher TPD capacities at lower TPD temperatures but SteamM7 had lower TPD capacities for all three hexane isomers by about 5% at higher TPD temperatures. It is evident that AcidM7 had a faster diffusion rate than SteamM7. Van Don *et al.* attributed the faster hexane uptake on acid treated H-mordenite to predominantly a shortened intracrystalline diffusion path length with respect to the diffusivity change.[36]

In addition, those TPD data infer that the 12-MR micropore of mordenite became wider by acid post treatment but it became narrower by steam treatment. The change of microporous structures should be due to a partial collapse of 12-MR micropore during dealumination. Upon acid treatment, framework aluminium was partially leached into an acid solution phase to create cracks inside the 12-MR micropores, so-called "defected 12-MR micropore". The defects can enlarge the pore opening of the 12-MR micropore. On the other hand, dealumination with steam treatment caused a partial removal of framework Al^{IV}

from 12-MR pores into extra-framework Al^{VI} on the mordenite solid phase, which partially plugged the 12-MR micropores giving reduced micropores.

On the other hand, both the SAR_{NMR} and Al^{VI} concentration of the BaseM7 sample decreased (Table 2). The NMR data indicates that during the base treatment, silica dissolution preferentially to alumina and realumination of Al^{VI} into the zeolite framework occurred simultaneously. Earlier, Liu *et al.* reported that realumination of Al^{VI} of dealuminated USY into a framework tetrahedral aluminium site occurs under hydrothermal conditions or KOH treatment.[37] Tao *et al.* reported that alkaline treatment initially developed mesopores from the boundary portion of MFI zeolites to the bulk, and prolonged treatment destroys the mesopores.[38] Recently, Jin *et al.* reported that NaOH treatment on ZSM-5 can cause desilication and dealumination simultaneously.[39]

The effect of base treatment on porous structures can vary with the parent sample and treating conditions by means of the relative rate of desilication and realumination.

BET isotherms (Table 2) indicated the average mesopore size of mordenite ranks in the order of AcidM7 << SteamM7 < M7 << BaseM7. On the other hand, the TPD peak temperatures of the tested samples, either with *n*-C_6 or DMB isomers, increased in the order AcidM7 < BaseM7 ~ M7 < SteamM7, implying the pore opening of 12-MR pore in reverse order. TPD capacities for all three hexane isomers in the BaseM7 sample were about the same as those in the parent M7 sample. The sorption data indicates that desilication by base treatment can generate a large mesopore size up to 7.0 nm and wider 12-MR pores, improving the diffusion property of BaseM7. The modified microporous structure of BaseM7 could be attributed to a partial collapse of the 12-MR micropore by base treatment by which framework silicon was partially leached into the base solution phase generating the so-called "defected 12-MR micropore". Similar to acid treatment but to a less extent, the defects enlarged the pore opening of 12-MR micropore of BaseM7. Coincidentally, all the post treated mordenite samples having lower Al^{VI} site percentage, such as AcidM7 and BaseM7, possessed enlarged 12-MR pores.

Regardless of variation in the framework SAR_{NMR} in the range studied, as shown in Table 2 and Fig. 5, all the parent M7 sample and post treated samples had about the same initial activity. The catalytic stability altered with post treatment methods followed the order of the much improved BaseM7 sample as the most stable one, the parent M7, then the deteriorated AcidM7 and the very poor SteamM7 as the fastest deactivated one. Previous studies showed that the effect of hierarchical pore structure on catalyst stability can be attributed to improved diffusion and more sparsely distributed aluminium sites.[7,40,41] Boveri *et al.*[7] reported that in the alkylation of benzene with 1-dodecene for linear alkylbenzene production, a post treatment procedure combining steam dealumination and acid washing can significantly improve the activity and stability of the parent mordenite sample. Wang *et al.* reported that the catalytic stability in naphthalene alkylation with *t*-butyl alcohol can by improved by acid treatment.[40] The improved performance was attributed to the increased mesoporous surface area, lower acid sites concentration and less hydrophilic surface. On the other hand, Srivastava *et al.* reported that hierarchical structure has a remarkable stabilization effect on the catalytic activity of mesoporous MFI zeolite.[41] The authors proposed that aluminium sparsely distributed in the mesopore walls in mesoporous MFI can retard coke formation. In another example, Li *et al.* reported that the activity of MFI in hexene aromatization could be accelerated and stabilized by NaOH post treatment.[42]

Accordingly, the alteration of the catalytic stability can be due to the changes of textural properties and framework structure associated with post treatment methods. As shown in Fig. 6, the catalytic stability of the parent M7 sample after dealumination became worse. As shown in Table 5, the residual aromatics on BaseM7 included TMB and dimethylethylbenzene (a transalkylation product of carbon number 10). The deteriorated stability could be attributed to the inhibited diffusion in the slightly smaller mesopore (5.4 nm) and partially plugged 12-MR pores of the SteamM7 sample, as discussed above. Some heavy alkylbenzene molecules, such as carbon number 10 molecules, were trapped inside the micropores of SteamM7, resulting in an acceleration in coke formation. As for the effect of dealumination by acid treatment, on one hand, the diffusion behavior of AcidM7 was improved by the so-called "defected 12-MR pore". On the other hand, the mesopore size of AcidM7 became narrower (4.4 nm). The catalytic stability of AcidM7 was only slightly poorer than that of the parent M7 sample, giving about the same line-out conversion but a much better one than SteamM7. Microporous structures could be more crucial to catalytic stability than mesopore structures. Referring to the porous structure of SteamM7, its mesopore size was only slightly lower; nevertheless, its deactivation was greatly accelerated due to partially plugged micropore structure by extra-framework Al^{VI}.

It is unprecedented that having enlarged mesopores up to 7.0 nm and defected 12-MR pores in BaseM7, the catalytic stability of the parent M7 sample was greatly improved by base treatment. As shown in Fig. 6, the catalyst stability of BaseM7 had been demonstrated exceeding a reaction period of 100 h. As shown in Table 5, the residual aromatics trapped inside the pores of BaseM7 were mainly TMB molecules with no carbon number 10 aromatic molecules found in SteamM7. The improved catalytic stability of BaseM7 sample could be attributed to the improved diffusion property in the meso-micro hierarchical structure. Thus, the textural property of zeolite samples significantly affects coke formation. Mesopores can be generated with various procedures to improve catalytic stability by facilitating the diffusion rate of reaction intermediate and desorption rate of products.

The state-of-the-art transalkylation of heavy alkylbenzenes technologies use exclusively metal/zeolite catalyst.[3–5] The metal on the zeolite catalyst catalyzes excessive aromatics hydrogenation and hydrocracking reactions leading to dwindling benzene product purity down below 90% (Table 4) and safety concerns about excessive reactor exothermia during startup (Table 6). Benzene product purity can be improved up to the industrial specification of 99.85% by some newly developed methods, such as dual bed catalyst system, on-line sulfiding, or pre-coking startup procedure to suppress metal activity.[24–26]

The greenness of various transalkylation processes is briefly evaluated in terms of green chemistry principles[43] in Table 6. The most crucial green element in applying Pt/zeolite catalyst

Table 6 Green process evaluation

Catalyst system	Mordenite	Pt/mordenite based process				Base treatment
Complementary method	No	On-line sulfiding	Pre-coking	Dual bed	Extraction	No
Energy consumption	Base	1	1.05	1.02	1.25	1
Hydrogen consumption	Base	1.25	1.25	1.30	1.25	1
Reaction temperature rise	2–5 °C	+ 50 °C	+ 150 °C	+ 350 °C	+ 350 °C	2–5 °C
Product rate	Base	1	1	0.85	1	1
Benzene purity	100%	>99.85%	>99.85%	>99.85%	>99.85%	100%
Catalyst cycle life	<1 year	>2 years	<2 years	>2 years	>2 years	>2 years
Special comments	Low stability	Sulphur corrosion	Less active	Less throughput	Energy intensive	Green process

systems is green principle 3 (less hazardous chemical syntheses). The exothermal heat of hydrogenation associating with high hydrogen consumption could cause a temperature rise in transalkylation reactors greater than 100 °C per aromatic ring saturation.[44] Pt/zeolite could catalyze excessive hydrogenation leading to a reactor temperature rise of more than 350 °C with serious concerns about reactor runaway. The presulfiding procedure by injecting trace sulphur compounds into reactor feed is a widely applied industrial practice. It can temporarily inhibit hydrogenation activity by formation of Pt–S bonds giving an improved benzene product purity and reducing the reactor temperature rise during startup within a reasonable range of 50 °C. However, sulphur injection into reactor systems is a cumbersome solution bringing additional safety concerns about metallurgy corrosion. The pre-coking startup procedure using severe conditions for short term artificial coking on metal function is an environmental solution. Nevertheless, the catalyst's stability is sacrificed by the novel startup procedure. On the other hand, dual bed catalyst system consisting of Pt/zeolite in the upper bed and H-zeolite in the bottom bed is a practical technical solution for selective cracking of naphthene compounds but requires a slightly additional hydrogen consumption with a sacrificed product rate. Extraction is an existing engineering solution which selectively extracts aromatics compounds from naphthene mixtures. Additional extractions increase the energy consumption by about 25%. In summary, in addition to heavy alkylbenzene transalkylation, incorporating platinum on zeolite can enhance the catalytic stability of zeolite by additional reaction routes of hydrogenation. Nevertheless, all the Pt/zeolite based catalyst systems inevitably suffer the side-effects associated with additional hydrogenation routes.

By a totally new approach, getting away from hydrogenation routes, the base post treatment method can significantly improve catalytic stability. Therefore, there is no naphthene byproduct formation in transalkylation, furnishing minimal hydrogen consumption and energy consumption (green principle 6), achieving the best benzene product purity and, more importantly, enhancing the reactor operation safety (green principle 3). This post treatment method is simple, effective and an environmentally benign solution for the conversion of heavy alkylbenzenes. This study has demonstrated the application of optimum micro-meso hierarchical porous structures for green catalysis.

5. Conclusion

The effects of various post treatments on the pore structure of mordenite were studied. It was found that mordenite can retain its framework structure after dealumination by acid treating or steam treating and desilication by base treatment. As confirmed by ^{27}Al NMR spectra, the acid treatment was more effective for dealumination than the steam treatment. It was observed that dealumination narrowed down the mesopore size. In addition, the acid treatment generated the more porous "defected 12-MR micropore" but the steam treatment caused partial plugging of Al^{VI} on micropores with a reduced micropore size. In comparison, base treated mordenite had faster diffusion rates than the acid treated one. On the other hand, base post treatment can simultaneously remove preferentially framework silica and re-insert extra-framework Al^{VI} into the mordenite structure. Desilication by base treatment generated a mesopore size up to 7.0 nm and defected 12-MR micropores.

All the parent mordenite and post treated samples had about the same initial activity in transalkylation of heavy alkylbenzenes. The fast deactivation rate of the parent mordenite sample became slightly faster with acid post treatment and was severely accelerated with the steam post treatment. Interestingly, the very stable activity of the base post treated mordenite has been demonstrated to be comparable to the platinum incorporated mordenite catalyst at a platinum loading of 700 ppm but with a much higher benzene product purity.

By BET measurements, temperature programmed desorption measurements along with residual aromatics analysis, the effect of the various post treatments on the catalyst stability is attributed to diffusion properties. Microporous structures could be more crucial for the catalytic stability than mesopore structures. The improved catalytic stability of the BaseM7 sample could be attributed to the improved diffusion in the meso-micro hierarchical structure.

Comparing to the state-of-the-art Pt/zeolite catalyst, the zeolite by base post treatment presented a simple, effective and green solution for heavy alkylbenzene transalkylation without reactor temperature runaway concerns to produce the best product purity requiring low hydrogen and energy consumption.

Acknowledgements

We would like to thank Dr S. B. Liu for his fruitful discussions and Dr S. J. Huang for his help on NMR analysis. We gratefully acknowledge the financial support from the National Science Council, Taiwan (NSC 96-2120-M-390-001).

References

1 T. C. Tsai, S. B. Liu and I. Wang, *Appl. Catal. A: Gen.*, 1999, **181**, 355.

2 J. Čejka and B. Wichterlová, *Catal. Rev.*, 2002, **44**(3), 375.
3 T. C. Tsai, W. H. Chen, S. B. Liu, C. S. Tsai and I. Wang, *Catal. Today*, 2002, **73**, 39.
4 J. H. Beech, R. J. Cimini, N. J. Rouleau and T. C. Tsai, *Aromatics*, 1999, **51**, 27.
5 S. H. Oh, S. I. Lee, K. H. Seong, Y. S. Kim, J. H. Lee, J. Woltermann, W. E. Cormier and Y. F. Chu, *Stud. Surf. Sci. Catal.*, 2003, **145**, 487.
6 S. van Donk, A. H. Janssen, J. H. Bitter and K. P. de Jong, *Catal. Rev.*, 2003, **45**(2), 297.
7 M. Boveri, C. Márquez-Álvarez, M. Ángel Laborde and E. Sastre, *Catal. Today*, 2006, **114**, 217.
8 Y. Tao, H. Kanoh, L. Abrams and K. Kaneko, *Chem. Rev.*, 2006, **106**, 896.
9 G. J. de A. A. Soler-Illia, C. Sanchez, B. Lebeau and J. Patarin, *Chem. Rev.*, 2002, **102**, 4093.
10 B.-L. Su, A. Vantomme, L. Surahy, R. Pirard and J.-P. Pirard, *Chem. Mater.*, 2007, **19**, 3325.
11 K. Egeblad, C. H. Christensen, M. Kustova and C. H. Christensen, *Chem. Maert.*, 2008, **20**, 946.
12 J. C. Groen, Louk A. A. Peffer, J. A. Moulijn and J. Pérez-Ramírez, *Micro. Meso. Mat.*, 2004, **69**, 29.
13 Łukasz Mokrzycki, B. Sulikowski and Z. Olejniczak, *Catal Lett.*, 2009, **127**, 296.
14 C. S. Cundy, M. S. Henty and R. J. Plaisted, *Zeolites*, 1995, **15**, 342.
15 M. Ogura, S. Shinomiya, J. Tateno, Y. Nara and M. Matsukata, *Chem. Lett.*, 2000, 882.
16 J. C. Groen, J. Perez-Ramirez and L. A. A. Peffer, *Chem. Lett.*, 2002, 94.
17 P. Y. Chao, S. T. Tsai, T. C. Tsai, J. Mao and X. W. Guo, *Topics Catal.*, 2009, **50**(1–2), 185.
18 S. T. Tsai, P. Y. Chao, T. C. Tsai, I. Wang, X. X. Liu and X. W. Guo, *Catal. Today*, 2009, DOI: 10.1016/j.cattod.2009.02.018.
19 P. Y. Chao, Y. Y. Chuang, G. H. Ho, S. H. Chuang, T. C. Tsai, C. Y. Lee, S. T. Tsai and J. F. Huang, *J. Chem. Edu.*, 2008, **85**(11), 1558.
20 M. Guisnet and P. Magnoux, *Appl. Catal.*, 1989, **54**, 1.
21 H. S. Cerqueira, P. Ayrault, J. Datka, P. Magnoux and M. Guisnet, *J. Catal.*, 2000, **196**, 149.
22 G. Engelhardt and D. Michel, *High-Resolution Solid-State NMR of Silicates and Zeolites*, Wiley, Chichester, 1987.
23 T. Wang, C. Tsai and S. T. Huang, *Ind. Eng. Chem. Res.*, 1990, **29**, 2005.
24 P. H. Chao, H. W. Lin, C. H. Chen, P. Y. Wang, H. T. Sei and T. C. Tsai, *Appl. Catal. A Gen.*, 2008, **335**, 15.
25 T. C. Tsai, P. H. Chao and W. L. Zeng, *Stud. Surf. Sci. Catal.*, 2007, **170B**, 1611.
26 S. T. Tsai, P. H. Chao, S. B. Liu and T. C. Tsai, *Stud. Surf. Sci. Catal.*, 2008, **174B**, 1183.
27 P. Kowalczyk, M. Jaroniec, K. Kaneko, A. P. Terzyk and P. A. Gauden, *Langmuir*, 2005, **21**, 10530.
28 M. Thommes, B. Smarsly, M. Groenewolt, P. I. Ravikovitch and A. V. Neimark, *Langmuir*, 2006, **22**, 756.
29 S. Z. Qiao, S. K. Bhatia and D. Nicholson, *Langmuir*, 2004, **20**, 389–395.
30 M. A. Uguina, J. L. Sotelo, A. Rodríguez, J. I. Gómez-Cívicos and J. J. Lázaro, *Sep. Purif. Technol.*, 2006, **51**, 72.
31 C. Y. Chen and S. I. Zones, *Microporous Mesoporous Mater.*, 2007, **104**, 39.
32 E. N. Gribov, G. Sastre and A. Corma, *J. Phys. Chem. B*, 2005, **109**, 23794.
33 R. M. Barrer, in: *Molecular Sieve Zeolites II, ACS Advances in Chemistry Series*, vol. 102, American Chemical Society, Washington, DC, 1971, p. 1.
34 E. García-Pérez, D. Dubbeldam, T. L. M. Maesen and S. Calero, *J. Phys. Chem. B*, 2006, **110**, 23968.
35 J. Dwyer, F. R. Fitch, F. Machado, G. Qin, S. M. Smyth and J. C. Vickerman, *J.C.S. Chem. Comm.*, 1981, 422.
36 S. van Donk, A. Broersma, O. L. J. Gijzeman, J. A. van Bokhoven, J. H. Bitter and K. P. de Jong, *J. Catal.*, 2001, **204**, 272.
37 D. S. Liu, S. L. Bao and Q. H. Xu, *Zeolites*, 1997, **18**, 162.
38 Y. S. Tao, H. Kanoh and K. Kaneko, *Adsorption*, 2006, **12**, 309.
39 F. Jin, Y. Cui and Y. Li, *Appl. Catal. A–Gen.*, 2008, **350**, 71.
40 Y. Wang, L. Xu, Z. Yu, X. Zhang and Z. Liu, *Catal. Comm.*, 2008, **9**, 1982.
41 R. Srivastava, M. Choi and R. Ryoo, *Chem. Comm.*, 2006, 4489.
42 Y. N. Li, S. L. Liu, Z. K. Zhang, S. J. Me, X. X. Zhu and L. Y. Xu, *Appl. Catal. A-Gen.*, 2008, **338**(1–2), 100.
43 P. T. Anastas and J. C. Warner, *Green Chemistry: Theory and Practice*, NY: Oxford University Press, 1998.
44 T. C. Tsai, S. B. Liu and I. Wang, *Catal. Survey Asia*, 2009, **13**(2), 94.

